LAWRENCE
LIVERMORE
NATIONAL
LABORATORY

LLNL-JRNL-678548

Tungsten dust impact on ITER-like plasma edge

R. D. Smirnov, S. I. Krasheninnikov, A. Yu. Pigarov, T. D. Rognlien

October 26, 2015

Physics of Plasmas

Disclaimer

Tungsten dust impact on ITER-like plasma edge

R.D. Smirnov[1,*], S.I. Krasheninnikov[1], A.Yu. Pigarov[1], T.D. Rognlien[2]

[1]*University of California San Diego, La Jolla, CA 92093, USA*

[2]*Lawrence Livermore National Laboratory, Livermore, CA 94551, USA*

Keywords: dust, tungsten, ITER, tokamak, plasma, modeling

PACS: 52.55.Fa, 52.25.Fi, 52.25.Vy, 52.40.Hf

[*]Corresponding author e-mail: rsmirnov@ucsd.edu

Abstract

The impact of tungsten dust originating from divertor plates on performance of edge plasma in ITER-like discharge is evaluated using computer modeling with the coupled dust-plasma transport code DUSTT-UEDGE. Different dust injection parameters, including dust size and mass injection rates, are surveyed. It is found that tungsten dust injection with rates as low as a few mg/s can lead to dangerously high tungsten impurity concentrations in the plasma core. Dust injections with rates of a few 10 mg/s are shown to have significant effect on edge plasma parameters and dynamics in ITER scale tokamaks. The large impact of certain phenomena, such as dust shielding by an ablation cloud and the thermal force on tungsten ions, on dust/impurity transport in edge plasma and consequently on core tungsten contamination level is demonstrated. It is also found that high-Z impurities provided by dust can induce macroscopic self-sustained plasma oscillations in plasma edge leading to large temporal variations of edge plasma parameters and heat load to divertor target plates.

1 Introduction

The issues related to boundary plasmas and plasma material interactions have recently attracted growing attention of fusion community due to expected increased power and duration of the fusion plasma discharges in next generation fusion devices, such as ITER, leading to very high stationary and intermittent plasma fluxes to plasma-facing components (PFCs), in particular, to divertor target plates. From this perspective, tungsten was selected as divertor plate material in ITER [1], taking into account its favorable mechanical and refractory properties, as well as low plasma sputtering yields and low levels of hydrogen fuel retention as compared to more chemically active materials, e.g. carbon. However, recent plasma exposure experiments [2-4] demonstrate that melting damage of tungsten PFCs, in particular of the plasma-exposed leading edges, can occur under intermittent heat loads relevant to large Edge Localized Modes (ELMs) and plasma disruption events in ITER. Normal tungsten PFCs operation under elevated temperatures with recurrent heat load increases due to plasma transients can lead to material fatigue and changes of its grain structure [5,6]. Moreover, sputtered material re-deposition and implantation of plasma ions into tungsten, in particular helium, can significantly modify its surface layer morphology [7-10]. All these processes are known to lead to formation of microscopic tungsten dust or droplets, which can be transported into the plasma as well as accumulate on surfaces inside the fusion vessel [11]. Dust events are routinely observed on modern tokamaks [11-15], most recently on JET tokamak with tungsten/beryllium ITER-like wall [16]. Transport and ablation of such dust in the boundary plasmas is an important mechanism of impurity contamination, which can potentially significantly affect fusion plasma operation [17-20]. The potential effects are particularly important for high-Z impurities, such as tungsten, because of their low plasma tolerated concentrations as a result of high radiative efficiency. Although it is very hard to evaluate the rate of dust production in ITER prior to its actual operation due to large variety and complexity of the dust formation mechanisms, extrapolation of the recent data from tungsten exposure experiments on QSPA-Kh50 plasma accelerator [21] suggests that the tungsten dust production rates by ELMs in ITER can be up to 1g/s. Thus, it is imperative to assess what impact produced tungsten dust can have on ITER plasma performance. The aim of the present paper is to study potential effects that injection of tungsten dust can have on edge plasmas, similar to ones that are envisaged in ITER tokamak, using computer modeling. Different sizes, as well as mass injection rates of tungsten dust are

simulated to evaluate the magnitude of produced effects on the plasma and the critical dust level that can seriously impact ITER performance.

2 Modeling of dust transport with DUSTT/UEDGE code

To assess an impact of high-Z material dust on ITER-like plasma edge we use coupled DUSTT/UEDGE code [19]. The DUSTT is a Monte-Carlo code that solves dust dynamics equations, describing motion, charging, heating, and ablation of dust grains in plasma, and performs statistical averaging of dust related parameters in plasma volume [22,23]. The UEDGE is multi-fluid multi-physics code used for simulating plasma and impurity transport in tokamak edge [24]. The two codes are iteratively coupled, such that plasma parameters simulated with UEDGE are provided to DUSTT code for dust transport modeling, which in turn outputs volumetric impurity source arising from dust ablation in the plasma to UEDGE. The iterations are repeated until a steady-state solution is obtained with a desirable precision of plasma parameters. The DUSTT/UEDGE coupled code was validated using 3D dust trajectories reconstructed from stereoscopic camera measurements on NSTX [19,25].

In the present paper the simulations are carried out on a computational grid representing ITER Scrape-Off-Layer (SOL), divertor, private flux, and core-edge regions, which cover magnetic flux surfaces from $\Psi_{norm} = 0.950$ at the core-edge boundary to $\Psi_{norm} = 1.035$ at the wall. The central core plasma is not modeled with the UEDGE fluid code here due to practical limitations on number of modeled tungsten ionization states and essentially unknown core anomalous transport coefficients of the tungsten impurity ions. The main plasma ion mass is set to 2.5 amu assuming that the plasma contains equal parts of deuterium and tritium. The simulated core heating power is 100 MW equally distributed between plasma electron and ion components. The hydrogen ion flux from the core on the core-edge boundary is set to 4.057×10^{22} s^{-1}. The cross-field plasma transport is simulated as anomalous and purely diffusive with the diffusivity coefficients 0.3 m^2/s for hydrogen and 0.5 m^2/s for impurity ions. The cross-field heat diffusivity coefficients for electrons and ions are set to 1.0 m^2/s. The recycling coefficients of hydrogen at the divertor plates and main wall are assumed to be 1.0 with the hydrogen pumping simulated at the ITER designated divertor locations. The tungsten impurity recycling

coefficients on the plates and wall are taken equal to 0.2. No other plasma impurities are simulated except tungsten sputtered and injected as dust from the divertor plates, providing an unseeded divertor plasma regime. In the simulations we followed tungsten ions with charge numbers of up to $Z_i = 20$ to achieve reasonable computational times with multi-fluid UEDGE code. The selected upper Z_i limit is close to average tungsten charge number at the corona equilibrium radiation maximum [26] occurring at $T_e \sim 1$ keV, which is above the maximum electron temperature simulated at the core-edge boundary. It is also assumed that there is no net flux of tungsten ions to the core through the boundary $\Psi_{norm} = 0.950$. Thus, we can reasonably model tungsten radiation losses in the edge plasma, which give us a lower limit of the total steady-state impurity radiation excluding the core region.

The dust production and ejection in ITER divertor are modeled with continuous flux of tungsten dust grains of radius $R_d = 1, 10,$ and 100 μm from the divertor target plates into the plasma with various dust mass injection rates, S, ranging from 1 mg/s to 300 mg/s. The dust injection flux is distributed on the inner and outer divertor plates proportionally to the simulated plasma heat load profiles across magnetic flux surfaces on the plates. This distribution mimics the non-uniform damage of divertor target material leading to dust production. The injected dust grains have cosine angular distribution of initial velocities with respect to the normal to the divertor plates surface with a Maxwellian distribution of speeds with average value of 10 m/s, which is typical by order of magnitude for ejection speeds of dust observed in tokamaks and QSPA experiments [15,27]. At present, the DUSTT/UEDGE code allows finding only steady-state solutions for coupled dust-plasma transport presuming continuous influx of injected dust grains. This limitation, however, is justified when dust grain injection events are sufficiently frequent to assume that any plasma disturbances produced by an individual grain are statistically smoothed over the plasma transport time scale.

As a dust grain quickly heats and evaporates in fusion plasmas, it is generally surrounded by a cloud of ablation material that shields the grain from plasma. The dust shielding by the ablation cloud is associated with particles collisional scattering, ionization, and radiative energy losses that can significantly affect plasma heat and particle fluxes to the dust grains, and thus impacts dust propagation in fusion plasma. It was found earlier that the shielding effects become important for grain sizes larger than some R_d^{max} dependent on dust material and plasma

parameters, which for tungsten dust in typical SOL plasma conditions was evaluated to be ~10 μm [28,29]. The currently employed in the DUSTT code model of dust charging and heating in plasma is based on the Orbital Motion Limited (OML) theory, which neglects the impact of plasma particle collisions in the ablation cloud. To represent the effects of shielding in the modeling an *ad hoc* shielding factor, γ, is used to reduce plasma fluxes to sufficiently large dust grains. Recent theoretical treatment of the shielding effects of high-Z material dust estimates $\gamma \sim 0.1$ for 10 μm tungsten dust in SOL plasmas [30]. In the present modeling, no shielding was assumed for $R_d = 1$ μm dust ($\gamma = 1.0$), while for $R_d = 100$ μm dust $\gamma = 0.1$ was used according to the theoretical shielding estimates, and for $R_d = 10$ μm both the shielded ($\gamma = 0.1$) and the unshielded ($\gamma = 1.0$) cases were run.

3 Impact of tungsten dust on edge plasma in ITER

3.1 Impurity radiation and plasma parameters

The importance of dust shielding is illustrated in Fig. 1, where radiation profiles of tungsten impurities in ITER divertor are shown for 60 mg/s of 10 μm dust injection cases without ($\gamma = 1.0$) and with ($\gamma = 0.1$) the shielding. One can see that in the case with shielding (Fig. 1b) the impurity radiation power is much larger in hot plasma regions near the separatrix and in the core, as compared to the unshielded case (Fig. 1a). This is due to the shielding allowing the injected dust grains propagate deeper into the hot plasma before their complete evaporation, leading to higher concentrations and stronger radiation of impurities in the plasma. For comparison, the simulated total impurity radiated power in the case with shielding of 46 MW is almost twice of 26 MW without the shielding. Ablation of shielded dust grains deeper in the plasma also leads to somewhat lower impurity radiation in colder plasma in the vicinity of the wall, as seen from comparison of Fig. 1(b) and (a).

The total tungsten radiated power normalized by the core heating power (100 MW) as function of the dust mass injection rate is shown in Fig.2 (a) for the four simulated dust injection scenarios. One can see in this figure that dust shielding plays a more important role in dust impact on plasma than dust size for a same dust mass injection rate. At the low injection rates of less than 10 mg/s of tungsten dust, the impurity radiated power scales linearly with the rate for

all the simulated dust parameters. At these rates, the shielding leads to ~4 times increase of the total radiated power for 10 μm dust. At ~10 mg/s for the shielded cases and ~30 mg/s for the unshielded one the impurity radiated power starts to level off indicating substantial dust impact on the edge plasma. With the injection of more than 100 mg/s of the shielded tungsten dust and more than half of the total heating power radiated by impurities, we observed signs of thermal plasma collapse in the simulations.

In Fig. 2b, the portion of the impurity radiation coming from the core-edge region inside the separatrix is plotted. For the comparatively small dust injection rates of less than 10 mg/s the contribution of the core-edge into total tungsten impurity radiation is ~45 %. At the higher rates the contribution of the core-edge to total impurity radiation increases. One can see that the start of saturation of the total impurity radiation power at the higher injection rates coincides with the increase of the part of the radiation from the core-edge. This is due to significant reduction of the plasma heat flux from the core-edge to SOL, caused by the radiation losses, which leads to a decrease of density and an increase of temperature of the core-edge plasma, as the core boundary heat flux and the cross field transport coefficients are fixed in the simulations.

The impact of dust injection on plasma parameters at the separatrix outer mid-plane point is shown in Fig. 3. Despite the growth of plasma temperature in the core-edge region at high dust injection rates, the electron temperature at the separatrix is almost unchanged for up to 300 mg/s of dust injection, as the electron parallel heat conduction starts to dominate heat transport, which is characterized by weak dependence of the temperature on the heat flux. The substantial edge plasma density and pressure reduction is observed to begin at ~10-30 mg/s when the significant radiative power losses in the edge lead to reduction of the heat flux and plasma recycling in the divertor. As a consequence, the reduction of plasma pressure and density is seen throughout the edge including the core-edge plasma, as was indicated above.

Approximately 50 % of the simulated tungsten ions in the core-edge plasma have $Z_i < 20$, which contribute ~40 % of the tungsten radiated power in this region. The simulated average charge number of tungsten impurities at the separatrix is $\bar{Z}_i \sim 15$ and in the divertor region $\bar{Z}_i < 10$. This reaffirms the choice of the maximum $Z_i = 20$ for modeling impact of tungsten impurities in the edge plasma.

3.2 Core contamination and impurity transport

The concentration of tungsten impurities relative to the hydrogen plasma density at the core-edge interface is shown in Fig. 4 as function of the dust injection rate. One can see that the core relative impurity concentration increases nearly linearly with the dust injection rate, except for the higher rates, >10-30 mg/s, where the increase is slightly faster than linear. As was mentioned above, the simulated core plasma density begins to decrease for dust injection rates >10-30 mg/s. Accordingly, the total quantity of the tungsten impurity ions in the core-edge plasma starts to level off at such rates, while being nearly proportional to the dust injection at the lower rates. As one can see in Fig. 4, the values of tungsten impurity relative concentration of $\geq 10^{-5}$, which can significantly limit ITER operational regimes to the point where ignition is not possible [31], are already reached at dust injection rates of order of a few mg/s for the larger, ≥ 10 μm, shielded dust grains. Recall that dust production from ELMs in ITER can be as high as 1 g/s according to the estimates from QSPA-Kh50 experiment data [21]. Such high tungsten dust injection rates would prevent normal plasma discharge operation in ITER.

As can be seen in Fig. 4, dust shielding by the ablation cloud significantly influences the quantity of tungsten impurities in the core-edge plasma produced by dust injection. Approximately a 3-fold increase of the core tungsten relative concentration is observed for the dust shielded cases ($\gamma = 0.1$) as compared to the unshielded ones ($\gamma = 1.0$). However, except the $R_d = 100$ μm case, practically no dust particles were observed to cross the separatrix. Thus, most of tungsten is delivered to the core by means of impurity ion transport, while dust transport determines the spatial distribution of impurity atom source provided by dust ablation in the SOL. As such, transport parameters of impurity ions in the edge plasma are also essential to determine core impurity contamination.

The simulations demonstrate that one of the most important transport mechanisms responsible for penetration of tungsten impurity ions to the core is the parallel thermal force, arising due to strong plasma temperature gradient in the tokamak edge. For instance, for the injection of 1 μm unshielded dust with 100 mg/s rate the test simulations with the both plasma ion and electron thermal force components intentionally switched off gives the relative tungsten impurity concentration of 4.5×10^{-6} at the core-edge interface, which is compared to 1.7×10^{-4} with the thermal force. Similarly, the total tungsten radiated power is 9.5 MW with 13 % of it from the

core-edge region in the former case, as compared to 31.7 MW and 46 % in the case with the thermal force.

The effect of dust injection on divertor operation is illustrated in Fig. 5, where the peak heat load on the divertor plates as function of the dust injection rate is shown. It is seen that the heat load is significantly reduced for the injection rates >30 mg/s on both the inner and outer plates. Due to substantial impurity radiation in the divertor region, as shown in Fig. 1, the plasma temperature and pressure in the divertor drops, which leads to plasma detachment observed near the inner divertor plate and may cause divertor thermal instability and discharge collapse at dust injection rates >100 mg/s [19,20]. Note that as there are no impurities other than those originated from the dust in the divertor in these simulations, the initial heat flux to the plates is high. With other impurities, such as nitrogen seeded in ITER divertor for heat load mitigation, the dust injection rates leading to detachment and thermal collapse can be lower than simulated.

At tungsten dust injection rates >30 mg/s, plasma oscillations are observed simultaneously with the reduction of the heat flux in the divertor. In Fig. 6 time variation of the total tungsten impurity radiated power is shown, demonstrating the plasma oscillations for different dust injection cases. Analysis of plasma parameters suggests that the self-sustained oscillations are driven by impurity radiation – plasma condensation instability in the SOL [32]. The plasma density, temperature and impurity radiation power vary significantly during the oscillations, especially in the vicinity of the X-point, where variation of plasma parameters can be several times in the magnitude. The thermal force on the impurity ions acts as a returning force facilitating the oscillations and preventing plasma collapse due to radiation-condensation instability in the range of dust injection rates, similarly to the thermal waves in impurity seeded plasmas [33]. The oscillations are thus associated with macroscopic non-linear interplay of plasma and impurity transport in the SOL rather than meso-scale turbulent plasma transport. Similar oscillations were observed in SOLPS simulations of ITER plasma with seeded nitrogen impurities in the divertor [34]. Such plasma oscillations producing periodic changes of SOL plasma parameters and the simulated variation ~10 % of the heat load to divertor plates can cause undesirable cyclic thermal load on plate material in ITER, which would lead to material damage and dust production even in regimes with suppressed ELMs.

4 Conclusions

The impact of tungsten dust injection from divertor plates on ITER-like plasma edge is simulated using the coupled dust-plasma transport DUSTT-UEDGE code. It is demonstrated that tungsten dust injection with rates as low as a few mg/s can lead to relative concentrations of tungsten impurities in the core-edge plasma exceeding $\sim 10^{-5}$ level, at which the operational space of ITER plasma is already significantly reduced. At the injections rates >30 mg/s, the impurities introduced by tungsten dust are found to considerably affect the edge plasma parameters due to substantial radiative power losses (up to ~60 % of the core heating power) both in the core-edge and divertor regions. This power loss can lead to divertor plasma detachment and eventually to thermal plasma collapse at dust injection rates >100 mg/s.

We demonstrate that both the dust ablation dynamics and the followed transport of the ablated tungsten impurities in edge plasma are essential for core contamination by dust-produced impurities. We find that tungsten impurities introduced in plasma by the dust injection with rates >30 mg/s lead to macroscopic self-sustained plasma oscillations, causing periodic variation of edge plasma parameters, radiative power losses, and heat flux to the divertor target plates. Our analysis indicates that the oscillations are driven by impurity radiation – plasma condensation mechanism, where the role of the force preventing radiative collapse is played by the parallel thermal force on impurity ions. The periodic changes of heat load to divertor PFCs produced by such oscillations, which can also be generated by other high-Z impurities in the ITER edge plasma, may lead to damage of the PFC material. Unlike to meso-scale plasma instabilities, e.g. ELMs, no mitigation method of such oscillations is readily available, as their generation mechanism is associated with macroscopic plasma/impurity transport.

The obtained results show that production of high-Z material dust in ITER scale tokamaks can severely impact fusion performance producing unacceptably large impurity concentrations in the plasma core and causing significant changes in edge plasma parameters and transport. Some aspects of the dust and impurity transport, such as dust shielding by an ablation cloud and the thermal force on impurity ions, which are complex and difficult to account for accurately, are found to have large effect on the dust production rates that will seriously compromise ITER

performance. This prompts further development and experimental validation of the improved transport models for reliable predictions of dust impact on plasma in future fusion devices.

Acknowledgements

This material is based upon work supported by the U.S. Department of Energy, Office of Science, Office of Fusion Energy Sciences, under Award Number DE-FG02-06ER54852 at UCSD and Contract Number DE-AC52-07NA27344 at LLNL.

References

[1] R.A. Pitts, S. Carpentier, F. Escourbiac, et al., *J. Nucl. Mater.* **438** (2013), S48.

[2] B. Lipschultz, J.W. Coenen, H.S. Barnard, et al., *Nucl. Fusion* **52** (2012), 123002.

[3] J.W. Coenen, V. Philipps, S. Brezinsek, et al., *Nucl. Fusion* **51** (2011), 083008.

[4] K. Krieger, T. Lunt, R. Dux, et al., *Phys. Scr.* **T145** (2011), 014067.

[5] Y. Ueda, J.W. Coenen, G. De Temmerman, et al., *Fusion Eng. Des.* **89** (2014), 901.

[6] J. Linke, T. Loewenhoff, V. Massaut, et al., *Nucl. Fusion* **51** (2011), 073017.

[7] T. Venhaus, R. Causey, R. Doerner, and T. Abeln, *J. Nucl. Mater.* **290-293** (2001), 505.

[8] S. Takamura, N. Ohno, D. Nishijima, and S. Kajita, *Plasma Fusion Res.* **1** (2006), 051.

[9] J. Roth, E. Tsitrone, A. Loarer, et al., *J. Nucl. Mater.* **390-391** (2009), 1.

[10] G. Federici, P. Andrew, P. Barabaschi, et al., *J. Nucl. Mater.* **313** (2003), 11.

[11] S.I. Krasheninnikov, R.D. Smirnov, and D.L. Rudakov, *Plasma Phys. Control. Fusion* **53** (2011), 083001.

[12] K. Narihara, K. Toi, Y. Hamada, et al., *Nucl. Fusion* **37** (1997), 1177.

[13] A.L. Roquemore, N. Nishino, C.H. Skinner, et al., *J. Nucl. Mater.* **363** (2007), 222.

[14] W.P. West, B.D. Bray, and J. Burkart, *Plasma Phys. Control. Fusion* **48** (2006), 1661.

[15] D.L. Rudakov, A. Litnovsky, W.P. West, et al., *Nucl. Fusion* **49** (2009), 085022.

[16] M. Sertoli, J.C. Flannegan, A. Cackett, et al., *Phys. Scr.* **T159** (2014), 014014.

[17] J. Winter and G. Gebauer, *J. Nucl. Mater.* **266** (1999), 228.

[18] J.P. Sharpe, D.A. Petti, and H.W. Bartels, *Fusion Eng. Des.* **63-34** (2002), 153.

[19] R.D. Smirnov, S.I. Krasheninnikov, A.Yu. Pigarov, et al., *J. Nucl. Mater.* **415** (2011), S1067.

[20] R.D. Smirnov, S.I. Krasheninnikov, A.Yu. Pigarov, et al., *Contrib. Plasma Phys.* **5**2 (2012), 435.

[21] V.A. Makhlaj, I.E. Garkusha, N.N. Aksenova, et al., *J. Nucl. Mater.* **438** (2013), S233.

[22] A.Yu. Pigarov, S.I. Krasheninnikov, T.K. Soboleva, and T.D. Rognlien, *Phys. Plasmas* **12** (2005), 122508.

[23] R.D. Smirnov, A.Yu. Pigarov, M. Rosenberg, et al., *Plasma Phys. Control. Fusion* **49** (2007), 347.

[24] T.D. Rognlien, J.L. Milovich, M.E. Rensink, G.D. Porter, *J. Nucl. Mater.* **196-198** (1992), 347.

[25] J. Nichols, A.L. Roquemore, W. Davis, et al., *J. Nucl. Mater.* **415** (2011), S1098.

[26] D.E. Post, R.V. Jensen, C.B. Tarter, et al., *Atom. Data Nucl. Data Tables* **20** (1977), 397.

[27] S. Pestchanyi, I. Garkusha, V. Makhlaj, and I. Landman, *Phys. Scr.* **T145** (2011), 014062.

[28] S.I. Krasheninnikov and R.D. Smirnov, *Phys. Plasmas* **16** (2009), 114501.

[29] B.T. Brown, R.D. Smirnov, and S.I. Krasheninnikov, *Phys. Plasmas* **21** (2014), 024501.

[30] S.I. Krasheninnikov "On ablation of large high-Z material dust grain in fusion plasma", *J. Nucl. Mater.* (to be published, 2014).

[31] T. Pütterich, R. Neu, R. Dux, et al., *Nucl. Fusion* **50** (2010), 025012.

[32] J.F. Drake, *Phys. Fluids* **30** (1987), 2429.

[33] D.Kh. Morozov and J.J.E. Herrera, *Phys. Rev. Lett.* **76** (1996), 760.

[34] A. Kukushkin, ITER Organization (private communication, 2014).

Figure captions

Fig. 1 The impurity radiation profiles in the ITER divertor for 60 mg/s, 10 μm tungsten dust injection with $\gamma = 1.0$ (no shielding) (a) and $\gamma = 0.1$ (b).

Fig. 2 The normalized tungsten radiation power (a) and part of the tungsten radiated power from the core-edge region (b) as functions of dust mass injection rate.

Fig. 3 The electron temperature (a) and density (b) at the separatrix outer mid-plane location as functions of dust injection rate.

Fig. 4 The relative concentration of tungsten impurities at the core-edge interface for the simulated dust injection scenarios.

Fig. 5 The peak heat load on the divertor plates as function of dust injection rate for the different simulated dust injection parameters.

Fig. 6 The time evolution of the total radiated power for the different dust injection parameters leading to plasma oscillations. (Color figure is available online.)

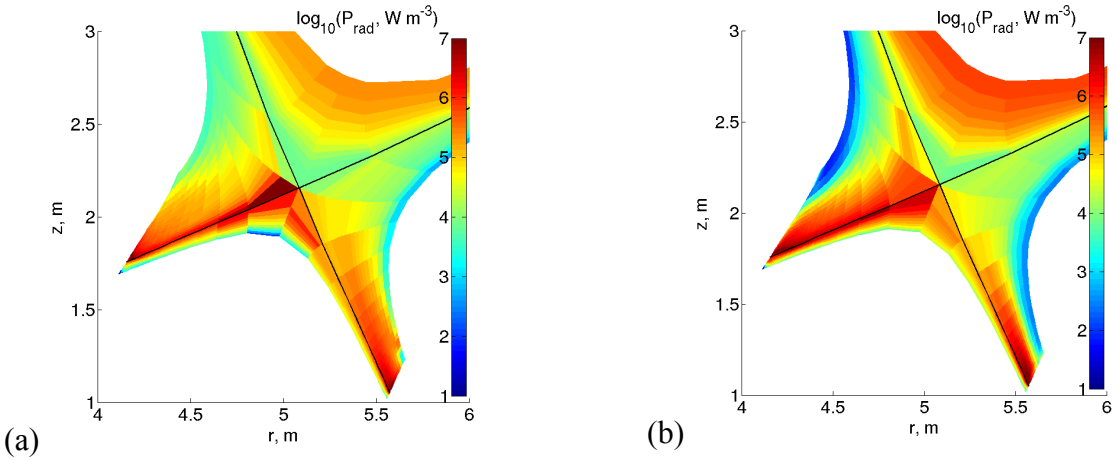

Fig. 1

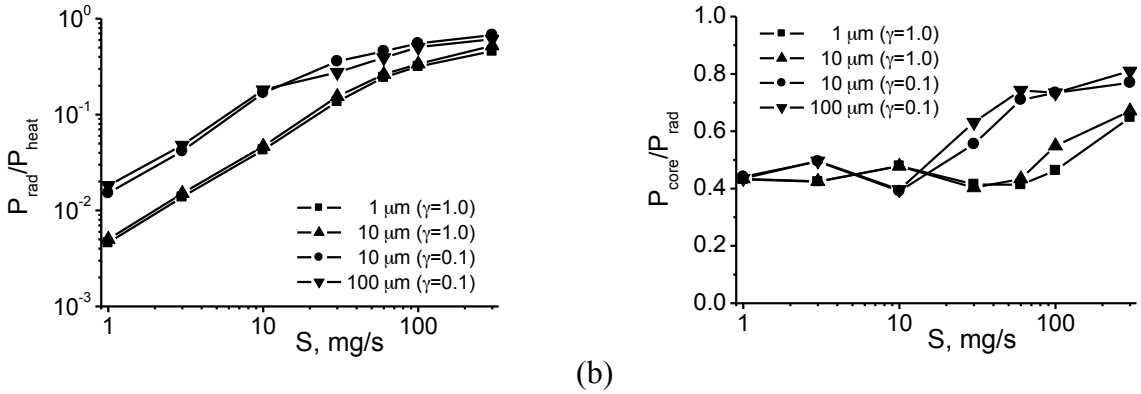
10^0
10^{-1}
10^{-2}
10^{-3}
P_{rad}/P_{heat}
1
10
100
S, mg/s
1 μm (γ=1.0)
10 μm (γ=1.0)
10 μm (γ=0.1)
100 μm (γ=0.1)
1.0
0.8
0.6
0.4
0.2
0.0
P_{core}/P_{rad}
1
10
100
S, mg/s
1 μm (γ=1.0)
10 μm (γ=1.0)
10 μm (γ=0.1)
100 μm (γ=0.1)

(a) (b)

Fig. 2

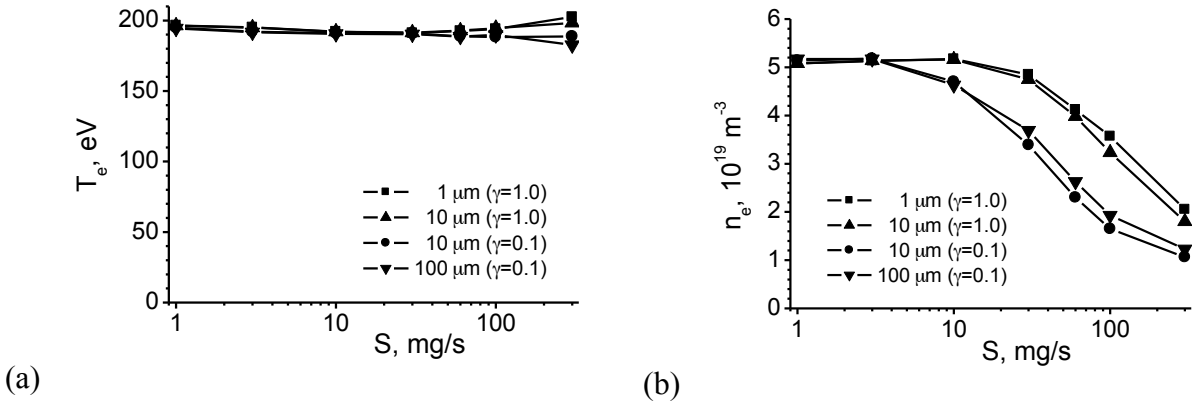
200
150
100
50
0
T_e, eV
1
10
100
S, mg/s
1 μm (γ=1.0)
10 μm (γ=1.0)
10 μm (γ=0.1)
100 μm (γ=0.1)
6
5
4
3
2
1
0
n_e, 10^{19} m^{-3}
1
10
100
S, mg/s
1 μm (γ=1.0)
10 μm (γ=1.0)
10 μm (γ=0.1)
100 μm (γ=0.1)

(a) (b)

Fig. 3

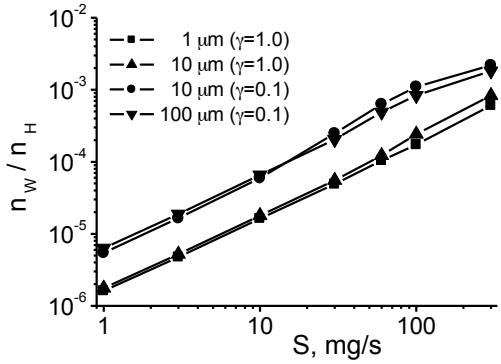
1 μm (γ=1.0)
10 μm (γ=1.0)
10 μm (γ=0.1)
100 μm (γ=0.1)
n_W / n_H
10^{-2}
10^{-3}
10^{-4}
10^{-5}
10^{-6}
1
10
100
S, mg/s

Fig. 4

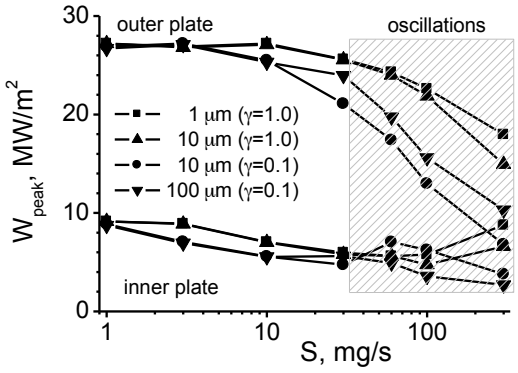
outer plate
oscillations
1 μm (γ=1.0)
10 μm (γ=1.0)
10 μm (γ=0.1)
100 μm (γ=0.1)
inner plate
W_peak, MW/m^2
S, mg/s
30
20
10
0
1
10
100

Fig. 5

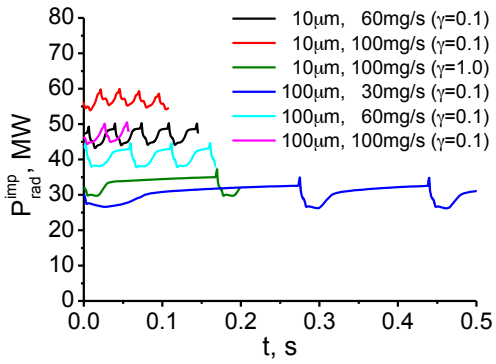
10μm, 60mg/s (γ=0.1)
10μm, 100mg/s (γ=0.1)
10μm, 100mg/s (γ=1.0)
100μm, 30mg/s (γ=0.1)
100μm, 60mg/s (γ=0.1)
100μm, 100mg/s (γ=0.1)
P_{rad}^{imp}, MW
t, s
0
10
20
30
40
50
60
70
80
0.0
0.1
0.2
0.3
0.4
0.5

Fig. 6